

## Research

# Three-dimensional Numerical Analysis of Contact Geometry in Back-contact Solar Cells

Hiroyuki Ohtsuka,<sup>1</sup> Yasuyuki Ohkura,<sup>2</sup> Tsuyoshi Uematsu<sup>1</sup> and Terunori Warabisako<sup>1</sup>

<sup>1</sup>Hitachi Research Laboratory, Hitachi Ltd., 7-1-1 Ohmika-cho, Hitachi-shi, Ibaraki 319-12, Japan

<sup>2</sup>Central Research Laboratory, Hitachi Ltd., 1-280 Higashi-koigakubo, Kokubunji-shi, Tokyo 185, Japan

*The device characteristics of back-contact solar cells, in which both p- and n-type contacts are integrated on the rear surface, are analyzed using a newly developed three-dimensional solar cell computing program. Comparing the characteristics of line- and point-contact models having the same contact area shows that, contrary to general expectation, the conversion efficiency of line-contact cells is higher than that of point-contact cells. Finally, the design criteria for achieving a conversion efficiency higher than 24% are discussed.*

## INTRODUCTION

The past decade has seen successful fabrication of single crystalline silicon solar cells exceeding the efficiency barrier of 20%.<sup>1-4</sup> One of these cells, a back-point-contact solar cell developed by Swanson *et al.*, has obtained an efficiency of 22.2% under AM1.5, 1 kW m<sup>-2</sup> sunlight.<sup>1</sup> As shown in Figure 1, this type of cell differs from conventional solar cells in that both p- and n-type contacts are arranged as an array of small dots on the back surface of the cell. This design yields a number of advantages: there is no shading of the front surface by contact grids; the illuminated front surface, which has a minimized diffused region, provides a very low surface recombination velocity; free carriers are generated in the lightly doped base, and hence long diffusion lengths of the minority carrier can be expected. Therefore, this design has been attractive as one candidate for achieving an efficiency of over 24%.

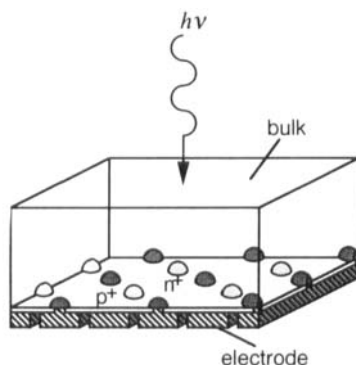


Figure 1. A schematic diagram of a back-point-contact solar cell

In order to raise the efficiency of a back-contact cell, it is important to optimize the geometry of diffusion regions and contacts. As a rule, the areas of diffusion regions and contacts in this type of cell have been regarded intuitively as being minimized towards the limit of point-contact size. However, as there have been few reports about the optimum design of such cells, except for a pseudo-three-dimensional (pseudo-3-D) analytical solution,<sup>5-7</sup> it remains in question whether the above assumption is correct. The pseudo-3-D solution cannot give a satisfactory answer to the issues of optimum conditions for diffusion regions and contact areas and shapes for this type of the cell. Needless to say, a simplified 1-D simulation cannot address the essential 3-D aspect of the problem and cannot treat the cell surface. Even 2-D simulation does not apply to point-contact cells because it cannot handle the contact shape.<sup>8</sup> Few 3-D simulations have been reported so far because computers do not always have enough power to execute such complex simulations.

The purpose of this study is to investigate the effect of the various shapes and sizes of diffused regions and contacts on the  $I-V$  characteristics of a back-contact solar cell. To make it possible to do 3-D calculations of solar cell characteristics, we developed several subroutines and combined them with the general purpose 3-D semiconductor device simulator CADDETH. This paper discusses the relationship between the contact design and  $I-V$  characteristics by comparing the characteristics of point- and line-contact cells with the same contact area. It also outlines the 3-D solar cell simulator that we developed.

## ANALYSIS

### Simulation method

In this study, we made it possible to calculate the solar cell characteristics of back-contact cells in three dimensions by revising a semiconductor device simulator (CADDETH).

The CADDETH (Computer Aided Device *DES*ign in *TH*ree dimensions) is a general purpose 2- and 3-D device modelling program developed by Hitachi, and simulates electrical characteristics of MOSFETs, bipolar transistors, p-n diodes and many other classes of devices.<sup>9</sup> The CADDETH performs DC analysis, AC analysis and transient analysis on them. A schematic diagram of the simulation flow is shown in Figure 2. In the first step, CADDETH accepts device geometries, doping profiles, bias conditions, mesh information, etc. In the next stage, it calculates simultaneously the following five basic semiconductor equations: Poisson's equation, continuity equations for electron and hole carriers and

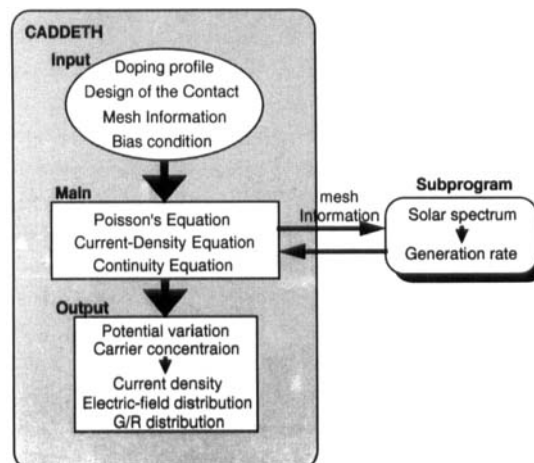


Figure 2. Simulation flow outline

current density equations for electrons and holes. As a result, the electrostatic potential,  $\psi$ , and the electron and hole concentrations,  $n$  and  $p$ , are solved. Using these data, CADDETH gives the terminal current density, the electric field distribution and the generation–recombination distribution.

The original CADDETH had a function for calculating the generation rate of electron–hole pairs by light illumination. However, it could not simulate solar cells because the function was limited to accepting incident light of only a single wavelength. Therefore, we modified the CADDETH to handle the spectral distribution of sunlight whose wavelength ranges from about 0.3  $\mu\text{m}$  to 4  $\mu\text{m}$ . Specifically, we developed a new subroutine program and attached it to the CADDETH. The new subprogram gives the photogeneration rate at a particular depth from the surface,  $x$ , by integrating the number of photons absorbed at  $x$  over all the wavelengths of the AM1.5 solar spectrum.<sup>10</sup> Here, the generation rate of electron–hole pairs generated by incident light is calculated by

$$G_{\text{Light}}(x) = \int \frac{\Phi_0(\lambda)}{h\nu} N(x, \alpha(\lambda)) \alpha(\lambda) \exp[-\alpha(\lambda)x] d\lambda \quad (1)$$

where  $\Phi_0(\lambda)$  is the illuminated photon flux,  $\lambda$  is the wavelength of incident light,  $N[\alpha(\lambda)]$  is the light-trapping coefficient,  $\alpha(\lambda)$  is the absorption coefficient,  $h$  is Planck's constant, and  $\nu$  is the frequency of photons. The absorption coefficient  $\alpha(\lambda)$  in Equation (1) is obtained from Rajkanan's equation.<sup>11</sup> The light-trapping coefficient  $N[x, \alpha(\lambda)]$  in Equation (1) is calculated from

$$N[x, \alpha(\lambda)] = (1 - R_{f_0}) \frac{1 + R_b \exp[-2\alpha(\lambda)(d - x)]}{1 - R_f R_b \exp[-2\alpha(\lambda)d]} \quad (2)$$

where  $R_{f_0}$  is the external reflectance of the front surface,  $R_f$  is the internal reflectance of the front surface,  $R_b$  is the internal reflectance of the back surface and  $d$  is the thickness of the cell. Note that the first term on the right describes the ratio of the transmitted light, and the second fractional term describes the ratio of absorbed light intensity with infinity times reflection to the transmitted light intensity. In this program, we assumed the generation efficiency of electron-hole pair is 100%, so the number of electron–hole pairs generated at a particular point in a solar cell is equal to the number of photons absorbed at that point.

The program ran on a supercomputer (HITAC S-820), using the Coupled Newton method to obtain the numerical solution. A typical run in simulating a  $50 \times 50 \times 75$  finite difference mesh and computing for about 20 bias points required at least half an hour of CPU time.

### Modelling parameters

Cross-sections of the unit cell used in the calculations are shown in Figure 3. This study examined both line-contact model (LCM) and point-contact model (PCM) types of back-contact cells. The simulated device consists of a 50- $\mu\text{m}$  thick p-type substrate with a resistivity of  $1.0 \Omega \cdot \text{cm}$  and a bulk lifetime of 1 ms. The peak surface doping concentration of  $1.0 \times 10^{20} \text{cm}^{-3}$  and a junction depth of 1.0  $\mu\text{m}$  with a complementary error function doping profile are assumed for both collector ( $p^+$ ) and emitter ( $n^+$ ). Here, the collector and emitter areas and the contact area in the LCM, which are 100  $\mu\text{m}^2$  and 25  $\mu\text{m}^2$ , respectively, are also assumed to be equal to those in the PCM. This assumption is required to investigate differences in characteristics caused by various contact geometries. So, calculations are also made for those LCMs that have very small emitter/collector and contact widths. The width of the unit cell, i.e. the pitch, is 50  $\mu\text{m}$ . The surface recombination velocity is assumed to be 100  $\text{cm s}^{-1}$ , as the surfaces of the cells are supposed to be passivated by  $\text{SiO}_2$  layers. The external reflectance is assumed to be 3% for a textured or antireflection-coated top surface. The internal reflectance of the top and bottom surfaces is assumed to be 92 and 98%, respectively.

The default values for the parameters used in computing the cell characteristics are listed in Table I, where an asterisk \* indicates the altered parameters appearing in Table II. The parameters used for our calculations are defined from the fabricated back-contact cell analysis. We chose a silicon substrate of much lower resistivity than that of the cells made by Swanson *et al.* to be supplied with high-quality

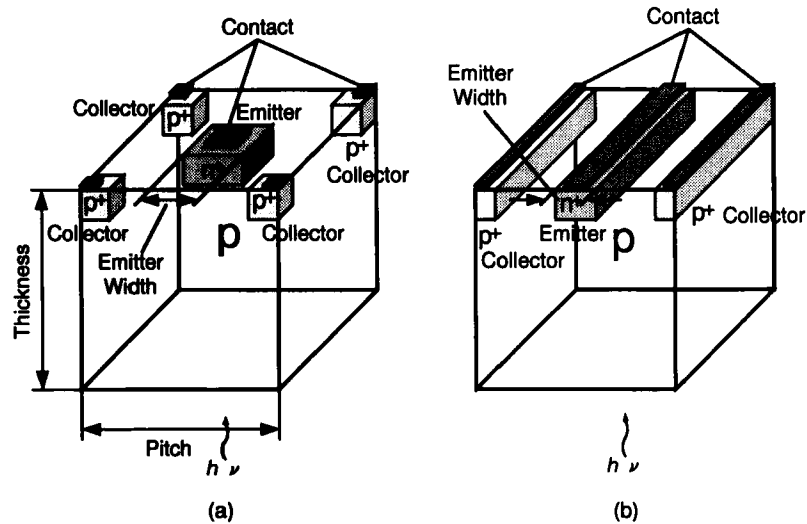


Figure 3. Simulation models of (a) a point-contact cell and (b) a line-contact cell: these are shown upside down so as to illustrate more clearly the electrode shapes. It is assumed that the diffusion and contact areas of the point-contact model are equal to those of the line-contact model

Table I. List of default geometric, material and performance parameters

Parameters	Input data
Thickness	50 $\mu\text{m}$
Pitch*	50 $\mu\text{m}$
Unit cell emitter area*	100 $\mu\text{m}^2$
Unit cell collector area*	100 $\mu\text{m}^2$
Unit cell contact area*	25 $\mu\text{m}^2$
Resistivity	1.0 $\Omega \cdot \text{cm}$
Surface doping concentration*	$1.0 \times 10^{20} \text{ cm}^{-3}$
Doping distribution	Complementary error function
Junction depth	1.0 $\mu\text{m}$
Surface recombination velocity*	100 $\text{cm s}^{-1}$
Lifetime*	1 ms
Surface reflection ratio	0.03
Inner reflection ratio (front side)	0.92
Inner reflection ratio (back side)	0.98
Temperature	298 K (25°C)
Intrinsic carrier concentration	$1.01 \times 10^{10} \text{ cm}^{-3}$
Sunlight	Global AM1.5, 1 $\text{kW m}^{-2}$

\* Altered parameters, see Table II.

Table II. Varied parameters used for calculation

Parameter	Input values
Pitch ( $\mu\text{m}$ )	25, 50, 100, 200, 400
Unit cell emitter/collector area ( $\mu\text{m}^2$ )	25, 36, 100, 196, 400
Surface impurity concentration ( $\text{cm}^{-3}$ )	$10^{18}$ , $10^{19}$ , $10^{20}$ , $5 \times 10^{20}$
Unit cell contact area ( $\mu\text{m}^2$ )	1.0, 6.25, 25, 100
Surface recombination velocity ( $\text{cm s}^{-1}$ )	0, 1, 10, 100, 200, 500, 1000
Lifetime ( $\mu\text{s}$ )	50, 100, 200, 500, 1000, 2000

wafers. But the choice of the lower resistivity wafers makes it necessary to etch them to 50  $\mu\text{m}$  thick because they have a shorter lifetime. Also, the range of these parameters was determined based on our real, fabricated cells.

Using the parameters in Tables I and II, an  $I$ - $V$  characteristics simulation was performed for both LCMs and PCMs, and the efficiency, open-circuit voltages and short-circuit currents were determined.

## RESULTS AND DISCUSSION

### Contact pitch dependency

Figure 4 shows the predicted efficiency ( $\eta$ ), open-circuit voltage ( $V_{oc}$ ) and short-circuit current density ( $J_{sc}$ ) for each model when the contact pitch is changed. The  $J_{sc}$  in both the LCM and the PCM decreases as the contact pitch increases. This is because the distance between the p-n junction and the carrier generation point becomes longer as the contact pitch does, thus increasing the carrier trapping rate due to the surface recombination and the Shockley-Read-Hall (SRH) recombination. For a pitch of 25  $\mu\text{m}$ , the difference between  $J_{sc}$  in the LCM and the PCM is not significant, but when it is 200  $\mu\text{m}$  the difference becomes quite large. There are two main candidates of the reasons for the difference. One is that the average distance between the p-n junction and the carrier generation point in the PCM becomes longer than that in the LCM as the pitch increases, i.e. the generation region L, whose points lie nearer a line contact than a point contact, becomes larger in the unit cell when the pitch increases, as indicated qualitatively in Figure 5. The other possibility is that when the pitch increases, the PCM suffers from the current concentration effect sooner than the LCM. The PCM has a region where the current vectors assemble, as shown in Figure 6. In this region, few carriers flow because of high resistance. As a result, the amount of surface recombination increases on the rear surface, i.e. this effect is more notable in the PCM than in the LCM as the pitch increases.

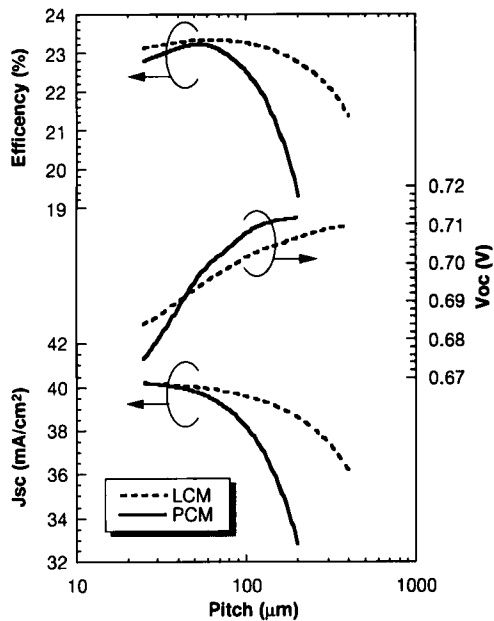


Figure 4. Efficiency,  $V_{oc}$ , and  $J_{sc}$  versus pitch for a line- and a point-contact cell: (—) point-contact model (PCM); (---) line-contact model (LCM)

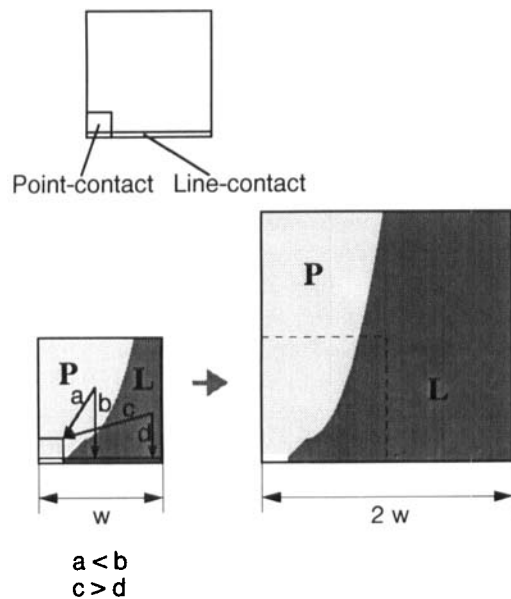


Figure 5. A sketch of the region near a point contact or a line contact: when the contact pitch is doubled, the region near the line contact is much larger than that near the point contact on the back surface of a unit cell

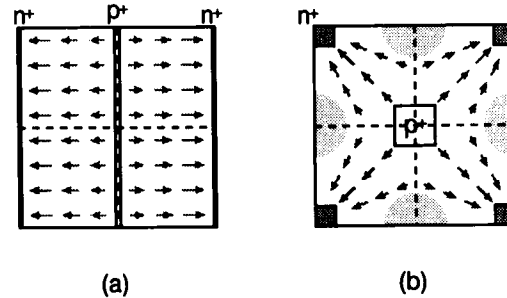


Figure 6. Illustration of the current vectors distributed on the backside for a line-contact cell (a) and a point-contact cell (b). The generated carriers cannot diffuse easily around the four shaded half-circles in a point-contact cell because the current vectors are not distributed uniformly like those of a line-contact cell

On the other hand,  $V_{oc}$  increases as the contact pitch increases, and at a faster rate in the PCM than in the LCM. This can be explained qualitatively by using the analogy of ideal  $I-V$  characteristics of p-n junction rectifiers of finite size with 'ohmic' end contacts (see the Appendix).<sup>1,2</sup> The p-type region spreads, becoming wider as the contact pitch becomes longer, and hence  $V_{oc}$  increases owing to the decrease in saturation current. The reason why the PCM's plot rises more steeply than the LCM's plot is that the distance between contacts in the PCM increases at the rate of  $\sqrt{2}$  times that in the LCM, so that the saturation current decreases more quickly in the PCM than in the LCM.

As a result, both the LCM and the PCM have a maximum  $\eta$  at 50  $\mu\text{m}$  pitch (corresponding to 4% diffusion coverage). At every pitch, the LCM's efficiency  $\eta$  is higher than that of the PCM. (The reason for this will be discussed later.) In particular, the efficiency in the PCM is quite low when the pitch is very short or very long, because of the lower  $V_{oc}$  or the lower  $J_{sc}$  of the PCM, respectively. These results point to the indispensability of pitch optimization using simulation when designing cell structures.

#### *Emitter/collector area and contact area*

Figure 7 shows the predicted  $\eta$ ,  $V_{oc}$  and  $J_{sc}$  when collector ( $p^+$ ) and emitter ( $n^+$ ) areas are altered. In both cases,  $J_{sc}$  increases as these areas become larger, although it is lower for the PCM than for the LCM. Although the absolute value of the difference between these models is small, the change is significant. On the other hand,  $V_{oc}$  decreases with increasing area. The reason for these trends is the same as in the case of contact pitch. Increasing the collector and emitter areas is almost equivalent to decreasing the pitch, except for the change in contact area. Consequently, the optimum emitter/collector area for a cell, the parameters of which are listed in Table I, is no more than 40  $\mu\text{m}^2$  (1.6% diffusion coverage) in the LCM and about 100  $\mu\text{m}^2$  (4% diffusion coverage) in the PCM.

Figure 8 shows the calculated dependency of  $\eta$ ,  $V_{oc}$  and  $J_{sc}$  on contact area. It shows that the  $V_{oc}$  in both cases decreases rapidly as the contact area increases. This is because carrier recombination increases with increasing contact area, where the surface recombination velocity is quite large due to the silicon-metal interface; as a result, the saturation current increases. The  $J_{sc}$  in both cases also decreases as the contact area increases because of the high rate of carrier recombination at the contact surface. Thus, the decreases in  $V_{oc}$  and  $J_{sc}$  cause the decrease in  $\eta$ .

It follows, then, that while the contact area should be as small as possible (of course, so far as the cell fabrication process permits), e.g. no more than 8  $\mu\text{m}^2$  in this case, the collector and emitter areas should not always be made small.

#### *Surface impurity concentration*

The dependencies of  $\eta$ ,  $V_{oc}$  and  $J_{sc}$  on the surface impurity concentration are shown in Figure 9. The  $J_{sc}$  in both models increases gradually with increasing concentration. The back-surface field (BSF) effect

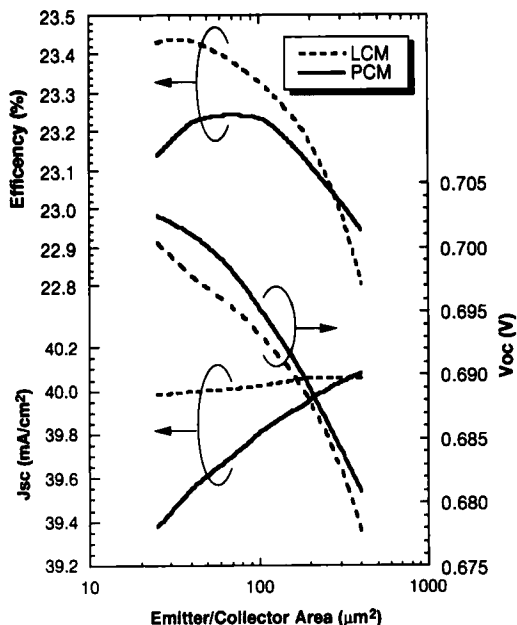


Figure 7. Efficiency,  $V_{oc}$ , and  $J_{sc}$  vs unit cell emitter/collector area

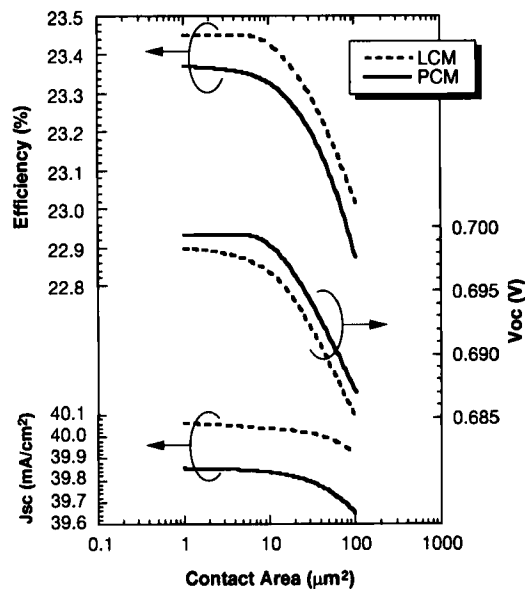


Figure 8. Efficiency,  $V_{oc}$ , and  $J_{sc}$  vs unit cell contact area

exerts a strong influence. In the region where the concentration is higher than  $1.0 \times 10^{19} \text{ cm}^{-3}$ ,  $J_{sc}$  saturates and then decreases. The decrease in the higher concentration range is attributed to the increasing Auger recombination rate in the collector and emitter regions. In the moderate concentration range,  $V_{oc}$  also increases because the saturation current decreases, owing to the increase of impurity concentration. In the concentration range higher than  $2.0 \times 10^{19} \text{ cm}^{-3}$ , the  $V_{oc}$  of the PCM begins to decline, indicating that the collector and emitter geometry of the PCM at high concentrations is less advantageous for obtaining high  $V_{oc}$  than that of the LCM. Consequently, the surface impurity concentration for the PCM has an optimum value of  $5.0 \times 10^{19} \text{ cm}^{-3}$ , while that for the LCM must be at least  $5.0 \times 10^{19} \text{ cm}^{-3}$  under the simulation conditions.

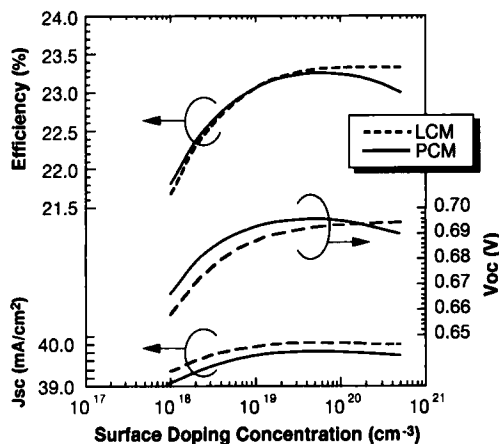


Figure 9. Efficiency,  $V_{oc}$ , and  $J_{sc}$  vs surface doping concentration

*Towards higher efficiency: surface recombination velocities and minority carrier lifetime*

Now let us look at design from the viewpoint of efficiency improvement. Figure 10 shows the predicted  $\eta$ ,  $V_{oc}$ , and  $J_{sc}$  plots when the minority carrier lifetime in the substrate is altered. As the lifetime increases, so do both  $J_{sc}$  and  $V_{oc}$ , and hence the efficiency increases. There is little difference between the  $V_{oc}$  plots for the LCM and the PCM. There is also little difference in the lifetime dependency of the two  $J_{sc}$  plots, while the absolute value for the LCM is higher than that for the PCM at any given lifetime. This means that the LCM is essentially better suited to collecting carriers than the PCM. All the current vectors of the LCM near the back surface have a certain magnitude and a regular direction, as shown in Figure 6(a). On the contrary, in the PCM there are stagnant areas, indicated by the four shaded half-circles in Figure 6(b), where the current vectors have negligible magnitude, so that the PCM collects fewer carriers than the LCM. We may, therefore, reasonably conclude that line-contact design should be adopted for a more efficient cell.

Figure 11 shows the predicted  $\eta$ ,  $V_{oc}$  and  $J_{sc}$  when the surface recombination velocity ( $S_0$ ) is changed: all drop markedly when  $S_0$  exceeds  $10 \text{ cm s}^{-1}$ . Recently, the substrate thickness tends to be thin in order to achieve higher  $V_{oc}$  (in this case, the substrate thickness is  $50 \mu\text{m}$ ), so that the cell characteristics are affected more strongly by the surface quality. The difference between the  $J_{sc}$  of the LCM and the PCM is very small for  $S_0 \leq 10 \text{ cm s}^{-1}$ , while for  $S_0 \geq 100 \text{ cm s}^{-1}$  the difference is significant. This supports the argument that in the PCM there are areas where surface recombination occurs more frequently because of the very small current vector. The  $V_{oc}$  of the PCM is lower than that of the LCM for  $S_0 \geq 200 \text{ cm s}^{-1}$ . This also indicates that the carriers recombine more easily in the PCM than in the LCM for very high  $S_0$ , because in the emitter/collector region in the PCM the carriers run for a longer distance than in the LCM. However, in the region of  $S_0 \leq 10 \text{ cm s}^{-1}$ , the  $\eta$  of the PCM is calculated to be higher than that of the LCM.

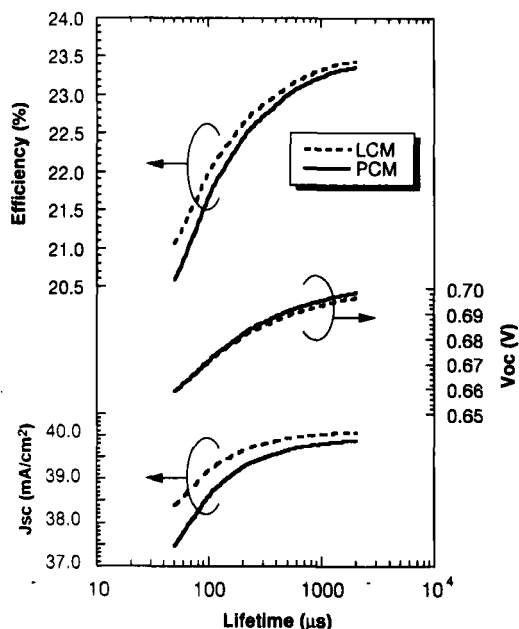


Figure 10. Efficiency,  $V_{oc}$ , and  $J_{sc}$  vs lifetime

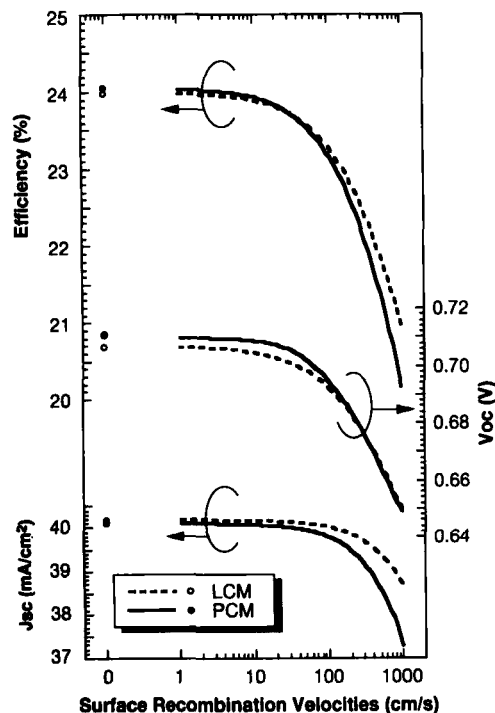


Figure 11. Efficiency,  $V_{oc}$ , and  $J_{sc}$  vs surface recombination velocities

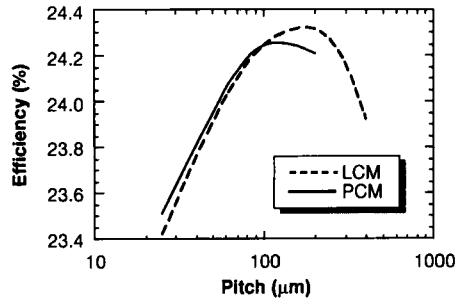


Figure 12. Variation of efficiency as a function of pitch for a line- and a point-contact cell with a surface recombination velocity of  $10 \text{ cm s}^{-1}$

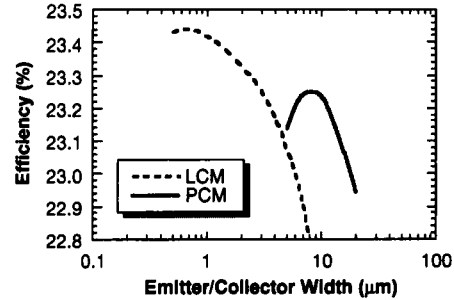


Figure 13. Efficiency vs emitter/collector width: emitter width is indicated in the sketch in Figure 3

Is it always true that  $\eta$  of the PCM is higher than that of the LCM for very low  $S_0$ ? The  $\eta$  dependence on pitch for the LCM and the PCM with a surface recombination velocity of  $10 \text{ cm s}^{-1}$  is shown in Figure 12. For a pitch of  $200 \mu\text{m}$ ,  $\eta$  in the LCM reaches 24.3% efficiency. Thus, the LCM indicates a conversion efficiency that is higher than that for the PCM even for very low  $S_0$  with varying pitch. Therefore, in order to design very high efficiency back-contact solar cells, we must make the contact linear, providing that the pitch or the diffusion area are optimized for the surface recombination velocity.

#### *Minimum emitter/collector width dependency*

Up to now we have been comparing the cell performance of LCM and PCM cells that have the same emitter/collector area. From now on we will discuss the case in which both models have the same emitter/collector width (ECW). This is because the minimum ECW is critical in the fabrication process.

Figure 13 shows the dependency of  $\eta$  on ECW, using the same data as for Figure 6. When the ECW is greater than  $5 \mu\text{m}$ , simulation shows higher  $\eta$  for the PCM than for the LCM. This is reasonable because the contact area in the PCM is much smaller than that in the LCM when both models have the same ECW. In this way, the highest efficiency obtainable using the feature size previously employed in solar cells is with a PCM design. But, the  $\eta$  of the LCM exceeds the maximum  $\eta$  of the PCM when the ECW is less than  $3 \mu\text{m}$ , i.e. an even higher efficiency can be obtained by using a very small feature size in an LCM design. Therefore, the LCM could be advantageous if the ECW could be set to  $3 \mu\text{m}$  or less.

## CONCLUSIONS

We have developed a solar cell device simulator by modifying a general purpose semiconductor device simulator, CADDETH, to simulate back-contact-type solar cells. With it, we have analysed the dependence of solar cell characteristics on the design and material parameters of point- and line-contact solar cells. This has led to three main conclusions:

- (i) In back-contact cells, the efficiency of the LCM is higher than that of the PCM when their emitter and collector areas are equal.
- (ii) To achieve a conversion efficiency higher than 24% in a back-contact-type cell, the emitter/collector and contact should be linear, provided that either the pitch or the diffusion area is optimized for the best surface recombination velocity. Also, the contact area should be as small as the cell fabrication process permits.
- (iii) The highest efficiency obtainable using the feature size previously employed in solar cells is with a PCM design. But an even higher efficiency can be obtained by using a very small feature size in an LCM design.

### Acknowledgements

This research was supported in part by the New Energy and Industrial Technology Development Organization as part of the Sunshine Project under the Ministry of International Trade and Industry. The authors wish to thank Dr H. Matsuo of Hitachi Central Research Laboratory for his guidance in using CADETH.

### APPENDIX

For an ideal p-n junction cell, the relation between  $V_{oc}$  and  $J_{sc}$  is given by

$$V_{oc} = \frac{kT}{q} \ln \left( \frac{J_{sc}}{J_0} + 1 \right) \quad (A1)$$

where  $k$  is Boltzmann's constant,  $T$  is the absolute temperature,  $q$  is the electron charge and  $J_0$  is the diode saturation current. As shown in Figure A1, when the diode structure is terminated by two free surfaces with surface recombination velocities  $S_e$  and  $S_h$ , the saturation current is calculated as

$$J_0 = Aqn_i^2 \left( \frac{D_e}{L_e N_A} F_p + \frac{D_h}{L_h N_D} F_N \right) \quad (A2)$$

where  $A$  is the cross-sectional area,  $n_i$  is the intrinsic carrier concentration,  $D_e$  and  $D_h$  are the respective diffusion coefficients for electrons and holes,  $L_e$  and  $L_h$  are the diffusion lengths for electrons and holes and  $N_A$  and  $N_D$  are the densities of acceptors and donors, respectively.<sup>12</sup> When  $S_e$  and  $S_h$  are both very large with respect to their characteristic diffusion velocities  $D_h/L_h$  and  $D_e/L_e$ , e.g. when the diode has metallic 'ohmic' end contacts,  $F_p$  and  $F_N$  have the form

$$F_p = S_e \coth \left( \frac{W_p}{L_e} \right) \quad (A3)$$

$$F_N = S_h \coth \left( \frac{W_N}{L_h} \right) \quad (A4)$$

where  $W_p$  and  $W_N$  are as defined in Figure A1.

The hyperbolic cotangent function  $\coth \theta$  is a monotonically decreasing function if  $\theta > 0$ . Moreover, if  $\theta \geq 2$ , then  $\coth \theta \approx 1$ .

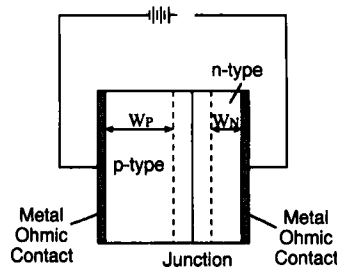


Figure A1. Geometry of a typical finite p-n rectifier with 'ohmic' end contacts that might be produced by an alloying or diffusion process

## REFERENCES

1. T. Saitoh, T. Uemats, Y. Kida, K. Matsukuma and K. Morita, 'Design and fabrication of 20%-efficiency, medium-resistivity silicon solar cells', *IEEE Electron Device Lett.*, **7**, 567–569 (1986).
2. R. A. Sinton and R. M. Swanson, 'An optimization study of Si point contact concentrator solar cells', *Proc. 19th IEEE Photovoltaic Specialists Conf.*, New Orleans, 1987, pp. 1518–1519.
3. A. Wang, J. Zhao and M. A. Green, '24% Efficient silicon solar cells', *Appl. Phys. Lett.*, **57**, 602–604 (1990).
4. J. Kopp, W. Warta, A. Aberle, S. Glunz and J. Knobloch, 'Impact of metallization techniques on 20% efficient silicon solar cells', *Proc. 22th IEEE Photovoltaic Specialists Conf.*, Las Vegas, 1991, pp. 278–283.
5. R. M. Swanson, 'Point contact solar cells: modeling and experiment', *Sol. Cells*, **17**, 85–118 (1986).
6. R. A. Sinton and R. M. Swanson, 'An optimization study of Si point contact concentrator solar cells', *Proc. 19th IEEE Photovoltaic Specialists Conf.*, New Orleans, 1987, pp. 1201–1208.
7. A. Luque, 'Analysis of high efficiency back point contact silicon solar cells', *Solid-State Electron.*, **31**, 65–79 (1988).
8. J. L. Gray and R. J. Schwartz, 'Why don't we have a 30% efficient silicon solar cell?', *Proc. 18th IEEE Photovoltaic Specialists Conf.*, Las Vegas, 1985, pp. 568–572.
9. T. Toyabe, H. Masuda, Y. Aoki, H. Shukuri and T. Hagiwara, 'Three-dimensional device simulator CADDETH with highly convergent matrix solution algorithms', *IEEE Trans. Computer-Aided Design*, **4**, 482–488 (1985).
10. *Measurement Principles for Terrestrial PV Solar Devices with Reference Spectral Irradiance Data*, International Electrotechnical Commission Standard 904-3. IEC (1989).
11. K. Rajkanan, R. Singh and J. Shewchun, 'Absorption coefficient of silicon for solar cell', *Solid-State Electron.*, **22**, 793–795 (1979).
12. J. P. McKelvey, *Solid State and Semiconductor Physics*, Harper & Row, New York, 1966.